

# Integration of Fullerenes as Electron-Acceptors in 3D Graphene Networks: Enhanced Charge Transfer and Stability Through Molecular Design

*Maira R. Cerón,<sup>a\*</sup> Cheng Zhan,<sup>a</sup> Patrick G. Campbell,<sup>a</sup> Megan C. Freyman,<sup>a</sup> Christy Santoyo,<sup>b</sup>  
Luis Echegoyen,<sup>b</sup> Brandon C. Wood,<sup>a</sup> Juergen Biener,<sup>a</sup> Tuan Anh Pham,<sup>a</sup> and Monika M.  
Biener.<sup>a\*</sup>*

<sup>a</sup> Materials Science Division, Lawrence Livermore National Laboratory, 7000 East Ave,  
Livermore, CA 94550, United States. <sup>b</sup> Department of Chemistry, University of Texas at El Paso,  
500 W University Ave, El Paso, TX 79968, United States.

KEYWORDS. 3D Graphene network, [60]fullerene, charge transfer, electrochemical stability.

**ABSTRACT.** Here we report a concept that allows the integration of the characteristic properties of [60]fullerene in 3D graphene networks. In these systems, graphene provides high electrical conductivity and surface area while fullerenes add high electron affinity. We use molecular design to optimize the interaction between 3D graphene networks and fullerenes, specifically in the context of stability and charge transfer in an electrochemical environment. We demonstrated that the capacity of the 3D graphene network is significantly improved upon the addition of C<sub>60</sub> and C<sub>60</sub> monoadduct by providing additional acceptor states in the form of the low lying LUMOs of C<sub>60</sub> and its derivative. Guided by experimental results and first-principle

calculations, we synthesized and tested a C<sub>60</sub> monoadduct with increased stability by strengthening the 3D graphene-C<sub>60</sub> Van-der-Waals interactions. The synthesis method and stabilization strategy presented here is expected to benefit the integration of graphene/C<sub>60</sub> hybrid materials in solar cell and charge storage applications.

**INTRODUCTION.** Graphene and fullerenes are examples of carbon nanomaterials with unique electronic structures and related electrochemical properties that have opened the door to many promising applications in the field of energy storage and harvesting.<sup>1</sup> Graphene combines high surface area with high electrical conductivity which makes it a promising supercapacitor and capacitive desalination material;<sup>1a,2</sup> fullerenes, on the other hand, are characterized by their high electron affinity which makes them excellent electron acceptors,<sup>3</sup> a property that has been exploited for photovoltaics.<sup>1b,4</sup> C<sub>60</sub> in particular has the ability to store up to 6 electrons in its energetically low lying, triply degenerated lowest unoccupied molecular orbital (LUMO) (that is, 0.1 electrons per carbon).<sup>3a,5</sup> For comparison, this is 5-10 times higher than the interfacial capacity of graphene (~0.01-0.02 electrons per carbon within the electrochemical stability window of water).<sup>2d,6</sup> In fact, the theoretical charge storage capacitance of [60]fullerene (223mAh/g) is similar or higher than that of today's standard lithium ion battery electrode materials (177 mAh/g for LiFePO<sub>4</sub>).

The challenge, however, is to make fullerenes electrochemically addressable which requires electrical wiring of individual fullerene molecules. Thus, integrating fullerenes with unique electron acceptor properties in 3D graphene networks with their high surface area and electrical conductivity would be of great benefit for many energy storage and harvesting applications. However, despite their significant potential technological benefits, there are only a few studies

about [60]fullerene-graphene hybrids,<sup>7</sup> including as electron extraction layers in polymer solar cells,<sup>8</sup> to enhance nonlinear optical performance,<sup>9</sup> as well as to facilitate exfoliation of graphite oxide to obtain graphene monolayers.<sup>10</sup> There is clearly a need to shed more light on design and synthesis strategies for graphene--fullerene nanocarbon networks, in order to take advantage of their unique electronic structure.

This work is aimed to achieve a fundamental understanding of the fullerene-graphene interface as it relates to electrochemical stability and charge transfer characteristics. Specifically, we designed, synthesized and tested a C<sub>60</sub> monoadduct that allowed us to significantly improve the electrochemical stability of fullerene functionalized-graphene. As an experimental platform, we used binder-free 3D mesoporous graphene macro-assemblies (GMAs) that have exceptionally high surface area (up to 1500 m<sup>2</sup>/g) and excellent conductivity (up to 100 S/m).<sup>11</sup> Using functionalized C<sub>60</sub> allowed us to increase the fullerene loading while reducing their tendency to cluster, and to increase the fullerene-graphene physisorption energy whereby increasing the electrochemical stability of the nanocarbon networks. Our experiments were guided by first-principle calculations that provided insights into the performance and stability of the hybrid electrodes.

**RESULTS AND DISCUSSION.** Cyclic voltammetry of C<sub>60</sub> physisorbed on the GMA electrodes<sup>11c</sup> (the preparation of the GMA-C<sub>60</sub> nanocarbon composites is described in the ESI) shows one C<sub>60</sub> related reversible redox wave (Fig. 1a, C<sub>60</sub> average loading 10 ± 3 wt%). To confirm that the redox wave observed between -0.8 and -1.1 V originates from the one-electron transfer to C<sub>60</sub>, we also measured the CV of C<sub>60</sub> in dichloromethane (Fig. 1a, black line, arbitrary units). While the redox peaks of both CVs are in qualitative agreement, we observed a 60 mV cathodic shift of the C<sub>60</sub> reduction peak that can be attributed to the characteristic timescale of

the charging kinetics of the bulk nanoporous GMA electrode. Although the fullerene loading is only 10%, the gravimetric peak current density of the GMA-C<sub>60</sub> electrode (Fig. 1a, orange line) increased by more than 50%, from 221.3 mA/g to 348.5 mA/g. The fraction of C<sub>60</sub> molecules that can be electrochemically assessed can be calculated by integrating the current peak associated with fullerene charging (Fig. 1a) and assuming a charge transfer of one electron per C<sub>60</sub> (subtracting the underlying GMA charging signal). This analysis reveals that 67% of the C<sub>60</sub> molecules in the GMA-C<sub>60</sub> electrodes can be electrochemically accessed (Fig 2S, see ESI); the fact that 33% of the deposited C<sub>60</sub> is electrochemically inaccessible suggests some cluster formation at a length scale below the SEM resolution. Note that these C<sub>60</sub> clusters must have formed during the impregnation as we used filtered C<sub>60</sub> solutions.<sup>12</sup>

In order to understand the capacitive performance of the GMA-C<sub>60</sub> electrodes, we carried out density functional theory (DFT) calculations of C<sub>60</sub> adsorbed on a single graphene sheet (representing GMA) using the Quantum-ESPRESSO code (see ESI). We focused on the high C<sub>60</sub> coverage regime, i.e., one C<sub>60</sub> per 60 graphene carbon atoms, that is relevant to the experimental condition. The difference in the charge storage behavior between hybrid and graphene electrodes can be assessed through the calculated electronic density of states (DOS) of the systems. As shown in Fig. 1b, the hybrid system exhibits an additional large peak in the DOS just above the Fermi level which is absent for pristine graphene. This peak originates from the triply degenerate LUMOs of the adsorbed C<sub>60</sub> molecule and explains for the experimentally observed redox wave between -0.8 and -1.1 V that improves the charge storage performance of GMA-C<sub>60</sub> at negative potentials. By contrast, C<sub>60</sub> does not induce new features in the occupied DOS within the indicated potential window, and hence little changes are expected in CVs towards the positive end of the potential sweep, in good agreement with the experiment (Fig 1a).

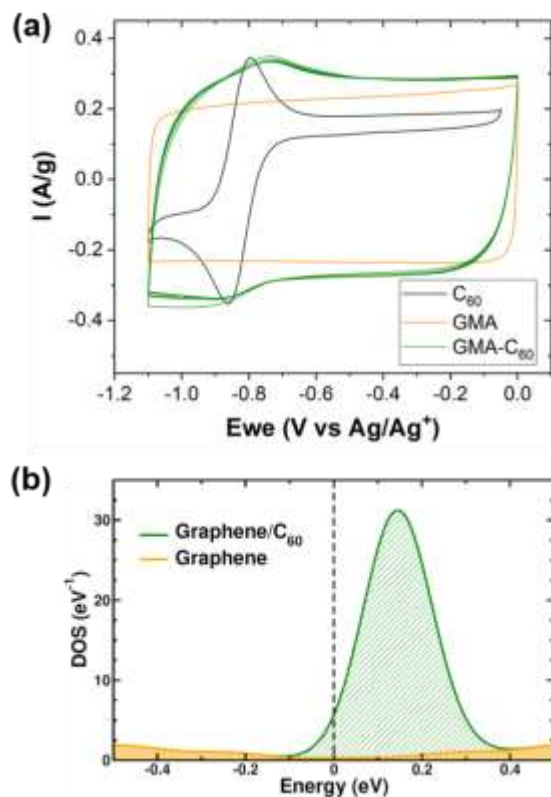


**Figure 1. (a)** Cyclic voltammogram of the first reduction peak of C<sub>60</sub> in dichloromethane (black line), GMA in acetonitrile (orange line) and GMA-C<sub>60</sub> in acetonitrile, 11.2% loading (green line). **(b)** Total electronic density of states of the graphene/C<sub>60</sub> electrode (black lines) computed for a model system consisting of one C<sub>60</sub> molecule and a graphene sheet of 60 carbon atoms. For comparison, the results computed for pristine graphene are also shown (orange lines).

Functionalization of fullerenes has been successfully used to increase their solubility, allow their characterization, and explore and tune their physical and chemical properties.<sup>4a, 13</sup> Specifically methanofullerene derivatives are well known for their thermal and electrochemical stability<sup>14</sup> and, as a result, they are often used for the fabrication of solar cells.<sup>4d, 15</sup> As described above, physisorption of C<sub>60</sub> on GMA resulted in low fullerene loadings ( $10 \pm 3$  wt%) and all attempts to increase the concentration of the C<sub>60</sub> solutions yielded cluster formation (it is

important to note that while C<sub>60</sub> clusters increase the loading they cannot be electrochemically addressed due to their large internal resistance).<sup>1c 12b</sup> To overcome this limitation, we synthesized a more soluble, less prone to cluster methanofullerene monoadduct. **PA-C<sub>60</sub>** was synthesized using a cyclopropane cycloaddition reaction from a diazo precursor, by *in-situ* base induced decomposition of 1-(4-aminophenyl)ethylidene-*p*-toluenesulfonyl hydrazide in the presence of C<sub>60</sub>, see ESI.

Physisorption of GMA with **PA-C<sub>60</sub>** resulted in average loadings up to  $29 \pm 4$  wt%, almost three times the loading achieved with C<sub>60</sub>. GMA-**PA-C<sub>60</sub>** loadings were confirmed by TGA. The TGA curves for a 27.5% GMA-**PA-C<sub>60</sub>** sample (Fig. 8S) showed a first weight loss at 200 °C corresponding to decomposition of the cyclopropane addend, followed by a weight loss starting at 500 °C corresponding to decomposition of the fullerene until reaching 1050 °C<sup>16</sup> where almost no mass loss is observed. Under our experimental conditions, the TGA curve of GMA-**PA-C<sub>60</sub>** showed a 47% total mass loss of the initial loaded fullerene, in agreement with the higher thermal stability of the monoadduct **PA-C<sub>60</sub>** compared to the pristine C<sub>60</sub> in which case almost all the initial loaded C<sub>60</sub> is lost (Fig. 3S). We also observed a higher decomposition temperature of the fullerene from 360 °C for the pure **PA-C<sub>60</sub>** to 500 °C for the hybrid GMA-**PA-C<sub>60</sub>**. This can be understood in view of the large number of wall contacts involved in diffusion through a bulk nanoporous material where even small changes in the van der Waals interaction can delay desorption through increasing the accumulative wall residence time.

CVs of GMA-**PA-C<sub>60</sub>** in the potential window from 0 to -1.3 V reveal that the position of **PA-C<sub>60</sub>** is negatively shifted compared to that for GMA-C<sub>60</sub> (Fig. 2a), consistent with previous reports of cathodic shifts upon double bond removal by chemical functionalization.<sup>17</sup> In addition, a good agreement was found between the CVs obtained from GMA-**PA-C<sub>60</sub>** and **PA-C<sub>60</sub>** in

dichloromethane, an indication that the observed redox wave originates from one-electron transfer into the C<sub>60</sub> monoadduct. The ~100 mV cathodic shift of the PA-C<sub>60</sub> reduction peak potential again reflects the characteristic charging kinetics of the bulk nanoporous GMA electrode. Remarkably, the functionalization with PA-C<sub>60</sub> doubles the gravimetric peak current density of the GMA electrode (Fig. 2a, orange line), from 272.2 mA/g to 548.6 mA/g. A detailed analysis reveals that, despite the high PA-C<sub>60</sub> loading, 82% of the physisorbed PA-C<sub>60</sub> molecules were electrochemically accessed (Fig. 1S, ESI). These results clearly demonstrate that functionalization of C<sub>60</sub> is an effective strategy to suppress cluster formation and increase the fullerene solubility.

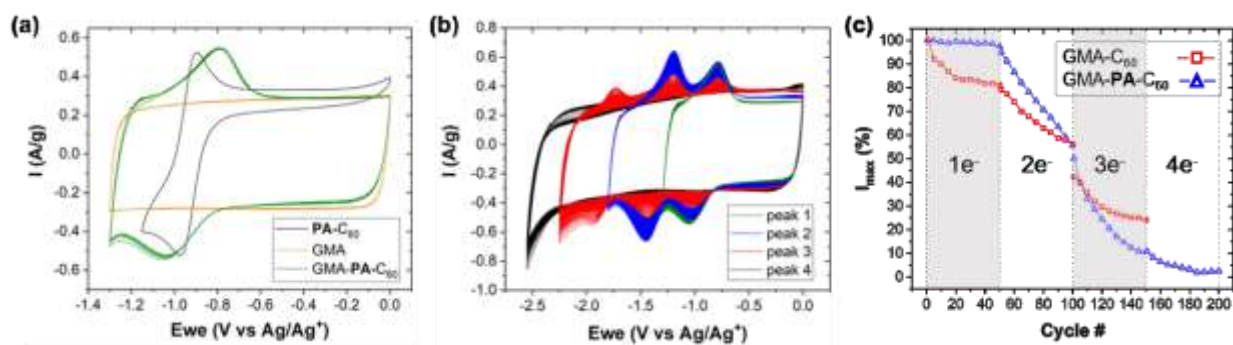


**Figure 2.** (a) Cyclic voltammogram of the first reduction peak of PA-C<sub>60</sub> in dichloromethane (black line), GMA in acetonitrile (orange line) and GMA-PA-C<sub>60</sub> in acetonitrile, 30.00% loading (green line). (b) Cycling voltammogram of GMA-PA-C<sub>60</sub> at different potential windows (c) Comparison of cycling stability of GMA-C<sub>60</sub> and GMA-PA-C<sub>60</sub>. The I<sub>max</sub> value is derived from CVs at different potential windows covering 1, 2, 3, or 4 electron transfers.

Cyclic voltammogram of GMA-PA-C<sub>60</sub> at different potential sweep rates allowed us to calculate the charge transfer utilization of GMA-PA-C<sub>60</sub> as a function of the scan rate (Figure 9S and 10S). We observed a slight decrease of the performance of GMA-PA-C<sub>60</sub> with increasing the

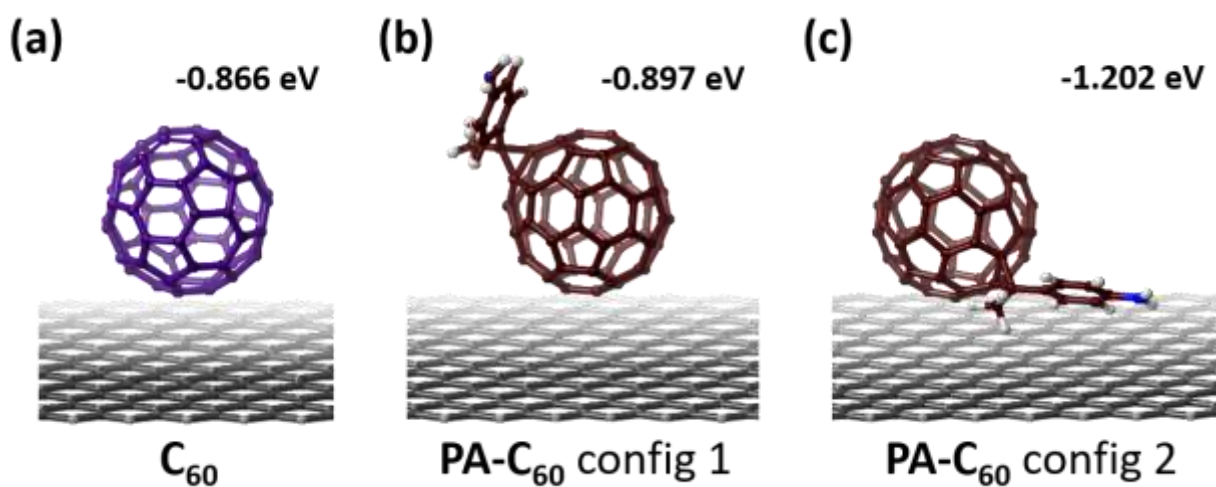
scan rate. The negative (cathodic) shift of the **PA-C<sub>60</sub>** related charging peak with increasing scan rate suggests that some solution resistance was not fully compensated thus preventing the complete charging of **PA-C<sub>60</sub>** at higher scan rates within the applied potential window.

Figure 2b/c shows a significantly higher cycling stability of **GMA-PA-C<sub>60</sub>** compared to **GMA-C<sub>60</sub>** when only 1 electron per fullerene molecule is introduced to the system. The electrochemical stability of physisorbed fullerenes depends, among other factors, on their solubility and the graphene-fullerene physisorption energy. The latter is expected to decrease with increasing electron transfer into the C<sub>60</sub> LUMOs, which leads to electrostatic repulsion between negatively charged graphene sheets and fullerene molecules (see discussion below). Interestingly, the stability trend **PA-C<sub>60</sub>** > **C<sub>60</sub>** observed for the first electron transfer (C<sub>60</sub> to C<sub>60</sub><sup>-</sup>) remains the same for the second electron transfer (C<sub>60</sub><sup>-</sup> to C<sub>60</sub><sup>2-</sup>) but is reversed for the third electron transfer (C<sub>60</sub><sup>2-</sup> to C<sub>60</sub><sup>3-</sup>). As demonstrated in a previous study,<sup>18</sup> the added negative charge is localized in the C<sub>60</sub> adsorbate. In this regard, the overall decreasing stability of physisorbed C<sub>60</sub> with increasing charge transfer can be qualitatively understood in terms of the increasingly repulsive interactions between the negatively charged C<sub>60</sub> adsorbate and the graphene substrate. Accordingly, accessing higher C<sub>60</sub> charging states (theoretically up to C<sub>60</sub><sup>-6</sup>) will require functionalization with more stable, covalently bonded C<sub>60</sub> derivatives.

Next, we calculated the binding energy of C<sub>60</sub> and **PA-C<sub>60</sub>** with the graphene substrate to investigate the stability of the fullerene-graphene hybrid electrodes. In particular, we performed classical molecular dynamics (CMD) to efficiently explore the most stable configurations of C<sub>60</sub> and **PA-C<sub>60</sub>** on graphene (see ESI).<sup>19</sup> These configurations were then re-optimized and used for binding energy calculations with DFT, which provides a more accurate description of molecular interactions in the systems. Analysis of the representative configurations (Fig. 3) derived from



CMD simulations shows that the functional group significantly enhances the bonding strength between PA-C<sub>60</sub> and graphene when being close to the substrate. This behavior stems from the  $\pi$ - $\pi$  interaction between the addend and graphene,<sup>20</sup> resulting in a 0.3 eV increase of the binding energy between PA-C<sub>60</sub> and graphene compared to that of C<sub>60</sub>. Collectively, these simulation results are consistent with TGA and CV measurements, indicating the important role of the functional group in determining the stability of the hybrid electrode.



**Figure 3.** Binding configurations of fullerene-graphene hybrids (a) C<sub>60</sub>-graphene. (b) PA-C<sub>60</sub>-graphene with the addend pointing away from the graphene. (c) PA-C<sub>60</sub>-graphene with the addend close to the graphene.

**CONCLUSIONS.** To summarize, we present a detailed investigation of the electrochemical charging behaviour of fullerene-graphene electrodes using a combination of experiments and first-principles calculations. When compared to pristine graphene, we find that the capacity of the system is significantly improved upon the addition of C<sub>60</sub> and C<sub>60</sub> monoadduct by providing additional acceptor states in the form of the low lying LUMOs of C<sub>60</sub> and its derivatives. We also showed that the design of the C<sub>60</sub> monoadduct plays a key role in the electrochemical

performance of the hybrid electrode. Specifically, increasing the solubility of C<sub>60</sub> which improved the C<sub>60</sub> loading and reduced cluster formation; the latter enhances the electrochemical accessibility of fullerene and thus warrants its utilization. Finally, functionalization of C<sub>60</sub> considerably improves the cycling stability of the hybrid material due to the additional  $\pi$ - $\pi$  interaction between the addend and graphene thus allowing access of charging states up to C<sub>60</sub><sup>3-</sup>. This trend was confirmed by DFT calculations of the binding energies of C<sub>60</sub> and C<sub>60</sub> monoadduct on graphene. The stabilization strategy presented in this work is ideally suited for applications that are dominated by one-electron transfer such as those in photovoltaic solar cells. Further optimization of the hybrid system using, e.g., covalently bonded fullerene-graphene, may provide even higher electrochemical stability thus benefiting energy storage applications.

#### ASSOCIATED CONTENT

**Supporting Information.** A detail description of the synthesis and characterization of fullerene derivatives and fullerene-3D graphene networks are listed in the ESI. As well as computational details.

#### AUTHOR INFORMATION

##### **Corresponding Author**

\*Dr. M. R. Cerón [ceronhernand1@llnl.gov](mailto:ceronhernand1@llnl.gov), \*Dr. M. M. Biener [biener3@llnl.gov](mailto:biener3@llnl.gov)

##### **Author Contributions**

The manuscript was written through contributions of all authors. All authors have given approval to the final version of the manuscript.

#### ACKNOWLEDGMENT

This work was performed under the auspices of the U.S. Department of Energy by Lawrence Livermore National Laboratory under Contract DE-AC52-07NA27344. Funding was provided by the Lawrence Livermore National Laboratory Directed Research and Development (LDRD) Grant 17-ERD-017. IM release: LLNL-JRNL-768044. Mass spectrometric measurements at the Molecular Foundry was supported by the Office of Science, Office of Basic Energy Sciences, of the U.S. Department of Energy under Contract No. DE-AC02-05CH11231. LE acknowledges the National Science Foundation, grants DMR-1205302, CHE-1408865 and CHE-1801317 for generous support. LE also thanks the Robert A. Welch Foundation for an endowed chair grant AH-0033.

#### ABBREVIATIONS

GMA, graphene macro-assemblies; LUMO, lowest unoccupied molecular orbital; SEM, scanning electron microscopy; vdW, van der Waals; TGA, thermogravimetric analysis; CV, cyclic voltammetry; DFT, density functional theory; CMD, classical molecular dynamics.

#### REFERENCES

1. (a) Jiang, H.; Lee, P. S.; Li, C., 3D carbon based nanostructures for advanced supercapacitors. *Energy Environ. Sci.* **2013**, *6* (1), 41-53; (b) Fang, Y.; Bi, C.; Wang, D.; Huang, J., The Functions of Fullerenes in Hybrid Perovskite Solar Cells. *ACS Energy Lett.* **2017**, *2* (4), 782-794; (c) Campbell, P. G.; Merrill, M. D.; Wood, B. C.; Montalvo, E.; Worsley, M. A.; Baumann, T. F.; Biener, J., Battery/supercapacitor hybrid via non-covalent functionalization of graphene macro-assemblies. *J. Mater. Chem. A* **2014**, *2* (42), 17764-17770.
2. (a) Simon, P.; Gogotsi, Y., Materials for electrochemical capacitors. *Nat. Mater.* **2008**, *7*, 845; (b) Gogotsi, Y.; Nikitin, A.; Ye, H.; Zhou, W.; Fischer, J. E.; Yi, B.; Foley, H. C.; Barsoum, M. W., Nanoporous carbide-derived carbon with tunable pore size. *Nat. Mater.* **2003**, *2*, 591; (c)

Zhang, L. L.; Zhao, X. S., Carbon-based materials as supercapacitor electrodes. *Chem. Soc. Rev.* **2009**, *38* (9), 2520-2531; (d) Yunpu, Z.; Yuqian, D.; Dongyuan, Z.; F., F. P.; T., M. R.; Sheng, D., Carbon Materials for Chemical Capacitive Energy Storage. *Adv. Mater.* **2011**, *23* (42), 4828-4850; (e) Simon, P.; Gogotsi, Y., Capacitive Energy Storage in Nanostructured Carbon–Electrolyte Systems. *Acc. Chem. Res.* **2013**, *46* (5), 1094-1103; (f) Hawks, S. A.; Knipe, J. M.; Campbell, P. G.; Loeb, C. K.; Hubert, M. A.; Santiago, J. G.; Stadermann, M., Quantifying the flow efficiency in constant-current capacitive deionization. *Water Res.* **2018**, *129*, 327-336; (g) Feng, X.; Zhao, J.; Sun, D.; Shanmugam, L.; Kim, J.-K.; Yang, J., Novel onion-like graphene aerogel beads for efficient solar vapor generation under non-concentrated illumination. *J. Mater. Chem. A* **2019**.

3. (a) Echegoyen, L.; Echegoyen, L. E., Electrochemistry of Fullerenes and Their Derivatives. *Acc. Chem. Res.* **1998**, *31* (Copyright (C) 2014 American Chemical Society (ACS). All Rights Reserved.), 593-601; (b) Guldi, D. M., Fullerenes: three dimensional electron acceptor materials. *Chem. Commun.* **2000**, (5), 321-327.

4. (a) Montellano Lopez, A.; Mateo-Alonso, A.; Prato, M., Chapter 11 Fullerenes for Materials Science. In *Fullerenes: Principles and Applications (2)*, The Royal Society of Chemistry: 2012; pp 389-413; (b) Hudhomme, P.; Cousseau, J., Chapter 12 Fullerene Derivatives for Organic Photovoltaics. In *Fullerenes: Principles and Applications (2)*, The Royal Society of Chemistry: 2012; pp 416-461; (c) Bianco, A.; Da Ros, T., Chapter 14 Biological Applications of Fullerenes. In *Fullerenes: Principles and Applications (2)*, The Royal Society of Chemistry: 2012; pp 507-545; (d) Mishra, A.; Bäuerle, P., Small Molecule Organic Semiconductors on the Move: Promises for Future Solar Energy Technology. *Angew. Chem. Int. Ed.* **2012**, *51* (9), 2020-2067.

5. (a) Ma, J.; Guo, Q.; Gao, H.-L.; Qin, X., Synthesis of C60/Graphene Composite as Electrode in Supercapacitors. *Fullerenes, Nanotubes and Carbon Nanostructures* **2015**, *23* (6), 477-482; (b) Kouloumpis, A.; Spyrou, K.; Dimos, K.; Georgakilas, V.; Rudolf, P.; Gournis, D., A Bottom-Up Approach for the Synthesis of Highly Ordered Fullerene-Intercalated Graphene Hybrids. *Front. Mater.* **2015**, *2* (10).
6. (a) Wood, B. C.; Ogitsu, T.; Otani, M.; Biener, J., First-Principles-Inspired Design Strategies for Graphene-Based Supercapacitor Electrodes. *J. Phys. Chem. C* **2014**, *118* (1), 4-15; (b) Stoller, M. D.; Magnuson, C. W.; Zhu, Y.; Murali, S.; Suk, J. W.; Piner, R.; Ruoff, R. S., Interfacial capacitance of single layer graphene. *Energy Environ. Sci.* **2011**, *4* (11), 4685-4689; (c) Ji, H.; Zhao, X.; Qiao, Z.; Jung, J.; Zhu, Y.; Lu, Y.; Zhang, L. L.; MacDonald, A. H.; Ruoff, R. S., Capacitance of carbon-based electrical double-layer capacitors. *Nat. Commun.* **2014**, *5*, 3317; (d) Zhan, C.; Neal, J.; Wu, J.; Jiang, D.-e., Quantum Effects on the Capacitance of Graphene-Based Electrodes. *J. Phys. Chem. C* **2015**, *119* (39), 22297-22303; (e) Paek, E.; Pak, A. J.; Hwang, G. S., A Computational Study of the Interfacial Structure and Capacitance of Graphene in [BMIM][PF6] Ionic Liquid. *J. Electrochem. Soc.* **2013**, *160*, A1-A10.
7. Guan, J.; Chen, X.; Wei, T.; Liu, F.; Wang, S.; Yang, Q.; Lu, Y.; Yang, S., Directly bonded hybrid of graphene nanoplatelets and fullerene: facile solid-state mechanochemical synthesis and application as carbon-based electrocatalyst for oxygen reduction reaction. *J. Mater. Chem. A* **2015**, *3* (8), 4139-4146.
8. (a) Tung, V. C.; Huang, J.-H.; Tevis, I.; Kim, F.; Kim, J.; Chu, C.-W.; Stupp, S. I.; Huang, J., Surfactant-Free Water-Processable Photoconductive All-Carbon Composite. *J. Am. Chem. Soc.* **2011**, *133* (13), 4940-4947; (b) Qu, S.; Li, M.; Xie, L.; Huang, X.; Yang, J.; Wang, N.; Yang, S., Noncovalent Functionalization of Graphene Attaching [6,6]-Phenyl-C61-butyric

Acid Methyl Ester (PCBM) and Application as Electron Extraction Layer of Polymer Solar Cells. *ACS Nano* **2013**, *7* (5), 4070-4081.

9. (a) Zhang, X.; Huang, Y.; Wang, Y.; Ma, Y.; Liu, Z.; Chen, Y., Synthesis and characterization of a graphene–C<sub>60</sub> hybrid material. *Carbon* **2009**, *47* (1), 334-337; (b) Liu, Z.-B.; Xu, Y.-F.; Zhang, X.-Y.; Zhang, X.-L.; Chen, Y.-S.; Tian, J.-G., Porphyrin and Fullerene Covalently Functionalized Graphene Hybrid Materials with Large Nonlinear Optical Properties. *J. Phys. Chem. B* **2009**, *113* (29), 9681-9686; (c) Zhang, X.; Liu, Z.; Huang, Y.; Wan, X.; Tian, J.; Ma, Y.; Chen, Y., Synthesis, Characterization and Nonlinear Optical Property of Graphene–C<sub>60</sub> Hybrid. *J. Nanosci. Nanotechnol.* **2009**, *9* (10), 5752-5756; (d) Ullmann, K.; Coto, P. B.; Leitherer, S.; Molina-Ontoria, A.; Martín, N.; Thoss, M.; Weber, H. B., Single-Molecule Junctions with Epitaxial Graphene Nanoelectrodes. *Nano Lett.* **2015**, *15* (5), 3512-3518; (e) Garrido, M.; Calbo, J.; Rodriguez-Perez, L.; Arago, J.; Orti, E.; Herranz, M. A.; Martin, N., Non-covalent graphene nanobuds from mono- and tripodal binding motifs. *Chem. Commun.* **2017**, *53* (92), 12402-12405; (f) Garcia, D.; Rodriguez-Perez, L.; Herranz, M. A.; Pena, D.; Guitian, E.; Bailey, S.; Al-Galiby, Q.; Noori, M.; Lambert, C. J.; Perez, D.; Martin, N., A C<sub>60</sub>-aryne building block: synthesis of a hybrid all-carbon nanostructure. *Chem. Commun.* **2016**, *52* (40), 6677-6680.
10. Zhang, Y.; Ren, L.; Wang, S.; Marathe, A.; Chaudhuri, J.; Li, G., Functionalization of graphene sheets through fullerene attachment. *J. Mater. Chem.* **2011**, *21* (14), 5386-5391.
11. (a) Worsley, M. A.; Pauzauskie, P. J.; Olson, T. Y.; Biener, J.; Satcher, J. H.; Baumann, T. F., Synthesis of Graphene Aerogel with High Electrical Conductivity. *J. Am. Chem. Soc.* **2010**, *132* (40), 14067-14069; (b) Worsley, M. A.; Olson, T. Y.; Lee, J. R. I.; Willey, T. M.; Nielsen, M. H.; Roberts, S. K.; Pauzauskie, P. J.; Biener, J.; Satcher, J. H.; Baumann, T. F., High Surface Area, sp<sup>2</sup>-Cross-Linked Three-Dimensional Graphene Monoliths. *J. Phys. Chem. Lett.*

**2011**, 2 (8), 921-925; (c) Worsley, M. A.; Kucheyev, S. O.; Mason, H. E.; Merrill, M. D.; Mayer, B. P.; Lewicki, J.; Valdez, C. A.; Suss, M. E.; Stadermann, M.; Pauzauskie, P. J.; Satcher, J. H.; Biener, J.; Baumann, T. F., Mechanically robust 3D graphene macroassembly with high surface area. *Chem. Commun.* **2012**, 48 (67), 8428-8430; (d) Biener, J.; Dasgupta, S.; Shao, L.; Wang, D.; Worsley, M. A.; Wittstock, A.; Lee, J. R. I.; Biener, M. M.; Orme, C. A.; Kucheyev, S. O.; Wood, B. C.; Willey, T. M.; Hamza, A. V.; Weissmüller, J.; Hahn, H.; Baumann, T. F., Macroscopic 3D Nanographene with Dynamically Tunable Bulk Properties. *Adv. Mater.* **2012**, 24 (37), 5083-5087.

12. (a) Ruoff, R. S.; Tse, D. S.; Malhotra, R.; Lorents, D. C., Solubility of fullerene (C<sub>60</sub>) in a variety of solvents. *J. Phys. Chem.* **1993**, 97 (13), 3379-3383; (b) Zhang, P.; Lu, J.; Xue, Q.; Liu, W., Microfrictional Behavior of C<sub>60</sub> Particles in Different C<sub>60</sub> LB Films Studied by AFM/FFM. *Langmuir* **2001**, 17 (7), 2143-2145.

13. (a) Hawkins, J. M.; Lewis, T. A.; Loren, S. D.; Meyer, A.; Heath, J. R.; Shibato, Y.; Saykally, R. J., Organic chemistry of C<sub>60</sub> (buckminsterfullerene): chromatography and osmylation. *J. Org. Chem.* **1990**, 55 (26), 6250-6252; (b) Caballero, R.; de la Cruz, P.; Langa, F., Chapter 3 Basic Principles of the Chemical Reactivity of Fullerenes. In *Fullerenes: Principles and Applications (2)*, The Royal Society of Chemistry: 2012; pp 66-124.

14. Cerón, M. R.; Izquierdo, M.; Aghabali, A.; Valdez, J. A.; Ghiassi, K. B.; Olmstead, M. M.; Balch, A. L.; Wudl, F.; Echegoyen, L., Tethered Bisadducts of C<sub>60</sub> and C<sub>70</sub> with Addends on a Common Hexagonal Face and a 12-Membered Hole in the Fullerene Cage. *J. Am. Chem. Soc.* **2015**, 137 (23), 7502-7508.

15. Thompson, B. C.; Fréchet, J. M. J., Polymer–Fullerene Composite Solar Cells. *Angew. Chem. Int. Ed.* **2008**, 47 (1), 58-77.

16. (a) Crumpton, D. M.; Laitinen, R. A.; Smieja, J.; Cleary, D. A., Thermal Analysis of Carbon Allotropes: An Experiment for Advanced Undergraduates. *J. Chem. Edu.* **1996**, *73* (6), 590; (b) Sundar, C. S.; Bharathi, A.; Hariharan, Y.; Janaki, J.; Sankara Sastry, V.; Radhakrishnan, T. S., Thermal decomposition of C<sub>60</sub>. *Solid State Commun.* **1992**, *84* (8), 823-826; (c) Cataldo, F., A STUDY ON THE THERMAL STABILITY TO 1000°C OF VARIOUS CARBON ALLOTROPES AND CARBONACEOUS MATTER BOTH UNDER NITROGEN AND IN AIR. *Fullerenes, Nanotubes and Carbon Nanostructures* **2002**, *10* (4), 293-311.
17. (a) Carano, M.; Marcaccio, M.; Paolucci, F., Three electrodes and a cage: an account of electrochemical research on C<sub>60</sub>, C<sub>70</sub> and their derivatives. *RSC Nanosci. Nanotechnol.* **2012**, *20* (Copyright (C) 2014 American Chemical Society (ACS). All Rights Reserved.), 237-269; (b) Kessinger, R.; Fender, N. S.; Echegoyen, L. E.; Thilgen, C.; Echegoyen, L.; Diedrich, F., Selective electrolytic removal of bis(alkoxycarbonyl)methano addends from C<sub>60</sub> bis-adducts and electrochemical stability of C<sub>70</sub> derivatives. *Chem. Eur. J.* **2000**, *6* (Copyright (C) 2013 American Chemical Society (ACS). All Rights Reserved.), 2184-2192; (c) Deng, F.; Wang, G.-W.; Zhang, T.-H.; Jiao, L.-J.; Chen, S., Ligand effects on the electrochemical and spectroscopic behaviors of methano[60]fullerene derivatives. *Chem. Commun.* **2004**, (9), 1118-1119.
18. Zhan, C.; Pham, T. A.; Cerón, M. R.; Campbell, P. G.; Vedharathinam, V.; Otani, M.; Jiang, D.-e.; Biener, J.; Wood, B. C.; Biener, M., Origins and Implications of Interfacial Capacitance Enhancements in C<sub>60</sub>-Modified Graphene Supercapacitors. *ACS Appl. Mater. Interfaces* **2018**, *10* (43), 36860-36865.
19. Ojeda-Aristizabal, C.; Santos, E. J. G.; Onishi, S.; Yan, A.; Rasool, H. I.; Kahn, S.; Lv, Y.; Latzke, D. W.; Velasco, J.; Crommie, M. F.; Sorensen, M.; Gotlieb, K.; Lin, C.-Y.;



Watanabe, K.; Taniguchi, T.; Lanzara, A.; Zettl, A., Molecular Arrangement and Charge Transfer in C60/Graphene Heterostructures. *ACS Nano* **2017**, *11* (5), 4686-4693.

20. (a) Li, K.; Li, H.; Yan, N.; Wang, T.; Zhao, Z., Adsorption and dissociation of CH<sub>4</sub> on graphene: A density functional theory study. *Appl. Surf. Sci.* **2018**, *459*, 693-699; (b) AlZahrani, A. Z., First-principles study on the structural and electronic properties of graphene upon benzene and naphthalene adsorption. *Appl. Surf. Sci.* **2010**, *257* (3), 807-810; (c) Zhang, Y.-H.; Chen, Y.-B.; Zhou, K.-G.; Liu, C.-H.; Zeng, J.; Zhang, H.-L.; Peng, Y., Improving gas sensing properties of graphene by introducing dopants and defects: a first-principles study. *Nanotechnology* **2009**, *20* (18), 185504.